MJFAS MALAYSIAN JOURNAL OF FUNDAMENTAL AND APPLIED SCIENCES
PRINT ISSN: 2289-5981 | ONLINE ISSN: 2289-599X

RESEARCH ARTICLE

High field carrier transport properties of $Al_{0.45}Ga_{0.55}N$

Wesley Ooi Tat Lung, Cheang Pei Ling, You Ah Heng*, Chan Yee Kit

Faculty of Engineering and Technology, Multimedia University, Jalan Ayer Keroh Lama, 75450 Melaka, Malaysia

**Corresponding author: ahyou@mmu.edu.my*

Article history
Received 13 September 2019
Revised 13 November 2019
Accepted 29 January 2020
Published 15 October 2020

Abstract

This work presented Monte Carlo (MC) simulation of $Al_{0.45}Ga_{0.55}N$ to investigate the carrier transport properties in the high electric field region including impact ionization. The simulation investigates both electron and hole considering two non-parabolic conduction band and valence band, respectively. The carriers' drift velocity, energy, and occupancy are simulated with respect to electric field at room temperature. The electron drift velocity peak at 2.70×10^7 cm/s with the electric field of 240 kV/cm. The electron starts to excite to higher valley at 170 kV/cm and has a spike in energy at 700 kV/cm due to the occurrence of impact ionization. The impact ionization rates are computed using modified Keldysh equation and it is shown that hole impact ionization rate is higher than that of electron for $Al_{0.45}Ga_{0.55}N$. This work also presents the impact ionization coefficient with hole dominating the impact ionization process above the electric field of 2.6 MV/cm.

***Keywords*:** Aluminium Gallium Nitride (AlGaN), avalanche photodiode, transport properties, impact ionization

INTRODUCTION

Wide-bandgap semiconductor materials have been researched as early as in the 1980s and it has been continued to mature until recent year. Materials such as Gallium Nitride (GaN) and Silicon Carbide (SiC) have been extensively studied and encouraging results have been reported. Ultra-wide-bandgap materials are the stages after wide-bandgap which the material has a larger bandgap than 3.4 eV of GaN. Those materials with bandgap larger than of GaN can benefit applications such as switching power conversion, pulsed power, RF electronics, Ultraviolet (UV) optoelectronics, and quantum information (Tsao *et al.*, 2017; Kaplar *et al.*, 2017). Besides, wide-bandgap semiconductor can contribute to UV radiation detection as UV detection is important for various civil and military applications such as chemical and biological analysis, flame detection, optical communications, emitter calibration, and astronomical studies (Monroy *et al.*, 2003).

Aluminium Gallium Nitride ($Al_xGa_{1-x}N$, $0 < x < 1$) avalanche photodiodes (APDs) usage for detection of light in UV regions has garnered great interests due to the properties of having low dark current, high optical gain, and high sensitivity (Huang *et al.*, 2013). Furthermore, AlGaN alloy has large direct band-gap energy (3.4 eV to 6.2 eV) while also having good chemical and thermal stability (Qu *et al.*, 1998). These properties combined with the solar-blind property of AlGaN for Al content above 40% make it a very good candidate for UV APD detection (Dong *et al.*, 2016).

AlGaN direct band-gap enables it to have high quantum efficiency which results in high gain. High gain is usually a result from the electron and hole impact ionization coefficient where one of the coefficients is larger than the other (Yuan *et al.*, 1999). Therefore, the performance of AlGaN is largely dependent on the impact ionization coefficient.

While numerous studies have been conducted on AlGaN, majority of those researches are about the gain and noise of the AlGaN, where the researchers are trying to optimize the gain of AlGaN with limited attention was paid to AlGaN transport properties especially AlGaN homostructure. The transport properties such as drift velocity, energy, and impact ionization coefficients are crucial to the performance of the AlGaN. This is due to higher electron saturation drift velocity can lead to higher performance of the material (Farahmand *et al.*, 2001) and the first spike in energy shows when the carrier starts to move to another valley as the electric field increasing whereas the second spike shows the impact ionization at higher electric field (El-Ela *et al.*, 2013). Furthermore, impact ionization coefficient is able to show the trend of the gain and excess noise of the APD (Bellotti *et al.*, 2014).

In order to get a better understanding on the carrier transport properties of the AlGaN APDs, Monte Carlo (MC) method was employed to develop a model to simulate the carrier transport properties (velocity, energy, carrier occupancy, impact ionization rate and coefficient for both electron and hole). The drift velocity, impact ionization rate, and coefficient were also compared with other previous studies.

MONTE CARLO SIMULATION

In the present work, both electron and hole transport properties were simulated together with two non-parabolic bands, respectively. The simulation began with setting the initial condition of the carrier by the process of selection of a random wave vector, $\vec{k}_x$. The carrier was then accelerated in the k-space during free flight by conservation of momentum (Tomizawa, 1993):

$$\overrightarrow{k_f} = \vec{k_i} + \frac{e\vec{F}\tau}{\hbar} \quad (1)$$

where $\overrightarrow{k_f}$ and $\vec{k_i}$ are final and initial wave vector respectively, F is the applied electric field, and $\hbar$ is the reduced Planck constant. The duration of free flight time, τ in each iteration was determined by

$$\tau = -\frac{\ln r}{\Gamma_o} \quad (2)$$

where r is the random number between 0 and 1 which represents the probability per unit time of a carrier scatters depending on the initial scattering rate Γ_o. For the initial condition of the simulation to have as little influence as possible on the final results, the total flight time had to be long. This flight time was used to calculate the velocity and the energy of the drift process. After the free flight process, any carrier containing energy greater than the band gap of the APD would scatter. During the scattering process, the wave vector was updated and the scattering mechanism was chosen. Using Fermi Golden's rule, the scattering mechanisms that were considered in this MC simulations were polar and non-polar optical phonon, acoustic phonon and impurity scattering. After each scattering process, the carrier's state and its wave vector after scattering were identified, then the scattering process is repeated until the end of the flight time. The simulation process was repeated under constant electric field up to the electric field of 1000 kV/cm to evaluate the drift motion.

Since AlGaN is a ternary alloy, the material parameters largely dependent on the percentage of Al where if the Al is 0%, the parameters will be that of GaN and 100% is that of Aluminium Nitride (AlN). Due to there being many percentages of Al content, the material parameters are not constant. There is a lack of definite knowledge on most of the parameters of $Al_{0.45}Ga_{0.55}N$ which necessitate the usage of linear interpolation obtained from the parameter of the binary parameter, GaN and AlN. The energy band gap however was deduced using the formula (Lee *et al.,* 1999; Zhang *et al.*, 2009; Dridi *et al.*, 2002; González *et al.*, 2008; Joachim, 2007)

$$E_g(x) = xE_g(AlN) + (1-x)E_g(GaN) - bx(1-x) \quad (3)$$

where $E_g(AlN)$ and $E_g(GaN)$ are the energy band gap of AlN and GaN respectively, x is the percentage of aluminium content, in this case 0.45 and b is the experimental bowing parameter. The bowing parameter differs from different researchers and some of the values from literature review are 0.62 (Lee *et al.,* 1999), 0.69 (Lee *et al.,* 1999), 1.3 (Angerer *et al.,* 1997), 0.75977 (Zhang *et al.*, 2009), 1.0 (Yun *et al.*, 2002), 0.71 (Dridi *et al.*, 2002), 1.3 (Stutzmann *et al.,* 1998) and 0.74 (González *et al.*, 2008). In this work, the bowing parameter was estimated to be 0.8 based on the consistent finding of bowing parameter above 0.7 (Joachim, 2007). The parameters of the $Al_{0.45}Ga_{0.55}N$ used in this simulation are linear interpolated (Coltrin *et al.*, 2017) and the result is as shown in Table 1.

During the simulation time t_{max}, the carrier mean drift velocity and average energy were simulated respectively with the formula (Tomizawa, 1993)

$$\vec{v} = \frac{\sum(E_f - E_i)}{q\overrightarrow{F_x}t_{max}} \quad (4)$$

and

$$E = \frac{\tau}{t_{max}}\sum\left(\frac{E_i + E_f}{2}\right) \quad (5)$$

where E_i is the carrier's energy at the beginning of the flight, E_f is the carrier's energy at the end of the flight, q is the charge of the carrier and $\overrightarrow{F_x}$ is the uniform electric field.

The impact ionization was categorized as a scattering mechanism and was represented in impact ionization rate and impact ionization coefficient. The impact ionization rate was modelled based on modified Keldysh equation (Keldysh, 1965; You *et al.,* 2008)

$$\frac{1}{\tau_i(E)} = P_i\left(E - E_{th}^i\right)^{\gamma_i} \quad (6)$$

where i is the band index, P_i is the softness coefficient, E_{th}^i is the ionization threshold energy, and γ_i is the power exponent. The material parameters used in this equation are listed in Table 2.

Table 1 Material parameters for wurtzite $Al_{0.45}Ga_{0.55}N$.

Carrier Type	Electron	Hole
Energy Band Gap (E_g) (eV, 300K)	4.46 [a, b]	4.46 [a, b]
Effective Mass (m_o) • First Valley • Second Valley	 0.26 [c] 1.23 [d]	 2.36 [c] 1.75 [c]
Dielectric Constant • Static relative permittivity (ε_o) • Optical relative permittivity (ε_∞)	 9.22 [c] 5.01 [c]	 9.22 [c] 5.01 [c]
Density (g cm^{-3})	4.84 [c]	4.84 [c]
Wave Velocity (m s^{-1})	9104 [c]	5071 [c]
Acoustic Deformation Potential (eV)	8.84 [c]	19.60 [c]
Polar Optical Phonon Energy (meV)	99.64 [c]	99.64 [c]
Energy separation between T and M-L valley) (eV)	1.36 [c]	0.006 [e]

[a]Lee *et al.*, 1999; [b]Zhang *et al.*, 2009; [c]Morkoç, 2008; [d]Bulutay, 2002; [e]Litvinov, 2003.

Table 2 Parameter for impact ionization rate for $Al_{0.45}Ga_{0.55}N$.

Carrier \ Parameter	i	P_i ($\times 10^{10}$ s^{-1})	E_{th}^i (eV)	γ_i
Electron	1	1	4.50	6
	2	2	4.55	6
Hole	1	1	4.65	7
	2	2	4.70	7

Impact ionization coefficients are the number of electron-hole pairs generated per unit distance traveled by a solitary carrier between two collisions. The coefficients were computed based on the number of times the carrier is scattered due to impact ionization. The coefficients are separated into electron (α) and hole (β) and is computed based on

$$\alpha = \left[\sum_{i=1}^{n_e} l_{ei} \Big/ n_e\right]^{-1} cm^{-1} \quad (7)$$

$$\beta = \left[\sum_{i=1}^{n_h} l_{hi} \Big/ n_h\right]^{-1} cm^{-1} \quad (8)$$

where n_e and n_h are the number of times the electron or hole scattered respectively while l_{ei} and l_{hi} are the travelling distance of electron and hole.

RESULTS AND DISCUSSION

In this study, MC method was applied with the parameters provided in Table 1 to simulate the velocity, energy, and the flight time of the carriers in $Al_{0.45}Ga_{0.55}N$. The impact ionization rates were simulated using modified Keldysh equation with the parameters shown in Table 2. The gain and noise of the APD were determined by the ratio between α and β, thus the α and β were simulated under various electric fields.

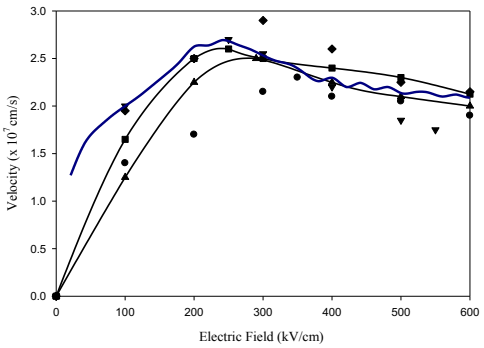

Fig. 1 $Al_{0.45}Ga_{0.55}N$ electron drift velocity as function of electric field of our work (solid line) compared to Anwar *et al.* (2001) ($Al_{0.4}Ga_{0.6}N$, circle), Bachir *et al.* (2012) ($Al_{0.4}Ga_{0.6}N$, square; $Al_{0.5}Ga_{0.5}N$, upright triangle), Yarar *et al.* (2010) ($Al_{0.5}Ga_{0.5}N$, inverted triangle), Farahmand *et al.* (2001) ($Al_{0.5}Ga_{0.5}N$, diamond).

Fig. 1 shows the comparison between our electron drift velocity with other researchers. As the drift velocity of homojunction $Al_{0.45}Ga_{0.55}N$ specifically cannot be found, it was compared with two closest percentage of Al content, which are $Al_{0.4}Ga_{0.6}N$ and $Al_{0.5}Ga_{0.5}N$. All the literature results are from simulation using MC methods as there is no experimental data for drift velocity on $Al_{0.45}Ga_{0.55}N$ so far. As shown in Fig 1, our result is comparable to various other researchers (Farahmand *et al.,* 2001; Anwar *et al.,* 2001; Bachir *et al.,* 2012; Yarar *et al.,* 2010). At a lower electric field, from 75 kV/cm to 170 kV/cm our result is close to the results from Yarar *et al.* (2010) and Farahmand *et al.* (2001). At a higher electric field, from 350 kV/cm to 600 kV/cm our result is in between Bachir *et al.* (2012) result from their $Al_{0.4}Ga_{0.6}N$ and $Al_{0.5}Ga_{0.5}N$ work which is agreeable compared to our $Al_{0.45}Ga_{0.55}N$. The difference in results might be due to the difference of the binary material parameters for AlGaN. The electron drift velocity in our work increases with electric field and achieves a maximum value of 2.70×10^7 cm/s at an electric field of 240 kV/cm. As the electric field increases, the electrons gain more energy and are excited to the higher valley where their effective mass increases. This increases the possibility of their collisions in the higher valley thus slowing them down. The further increase in the electric field beyond 500 kV/cm results in the saturation of the electron drift velocity at 2.10×10^7 cm/s.

Fig. 2 plots the average electron energy as a function of electric field for $Al_{0.45}Ga_{0.55}N$ in our work. At a lower electric field, below 170 kV/cm, the average electron energy remains low due to the electrons losing all the energy gained from the electric field through polar optical phonon scattering. After the 170 kV/cm point, the average electron energy increases exponentially. This is due to the excessive energy from the electric field where the polar optical phonon scattering mechanism is unable to absorb and therefore other scattering mechanisms start to happen (El-Ela *et al.*, 2013). The average electron energy at this point increases almost linearly to increasing electric field. The average electron energy increases exponentially at electric field greater than 700 kV/cm with the average electron energy of 3.6 eV from the occurrence of impact ionization.

The occupancy of electron as a function of electric field for our $Al_{0.45}Ga_{0.55}N$ model shows in Fig. 3. These electrons are completely occupied in the first energy valley when the electric field is below 170 kV/cm. When the electric field is above 170 kV/cm, the electron obtained sufficient energy from the electric field and begin to move towards the higher valley. The occupancy of electron at the first valley decreases to 40% while the electron at the second valley increases to 60% at electric field greater than 560 kV/cm. These shows that at high electric field, electrons are moving from the lower energy valley to the higher energy valley and the ratio of 40-60 is kept at saturation.

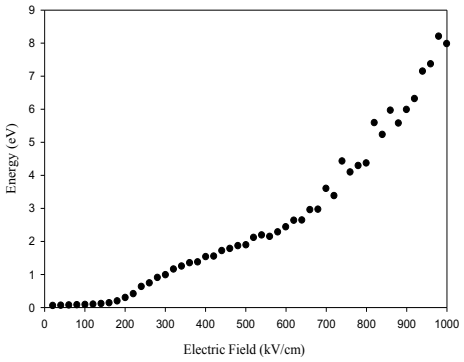

Fig. 2 $Al_{0.45}Ga_{0.55}N$ electron energy as function of electric field.

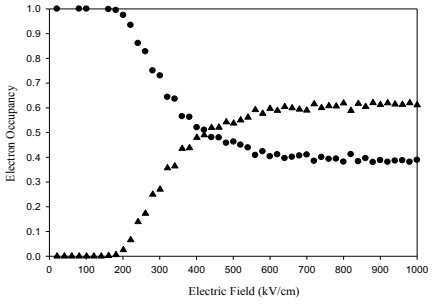

Fig. 3 $Al_{0.45}Ga_{0.55}N$ electron occupancy as function of electric field. Circles: Occupancy of electron at first valley. Triangles: Occupancy of electron at second valley.

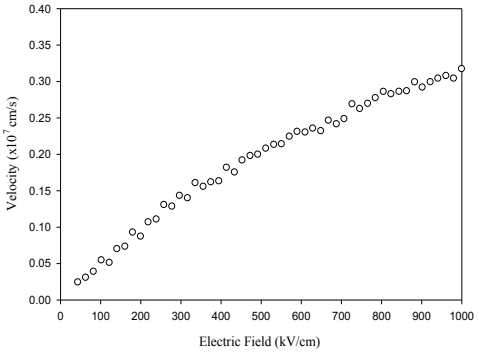

Fig. 4 $Al_{0.45}Ga_{0.55}N$ hole drift velocity as function of electric field.

Fig. 4 shows the hole drift velocity simulation of $Al_{0.45}Ga_{0.55}N$ as a function of electric field. To date, there is no data on the hole drift velocity of $Al_{0.45}Ga_{0.55}N$ experimentally or from simulation available from other researchers. At 500 kV/cm, the hole velocity is 2.0×10^6 cm/s which is less than a tenth of the electron drift velocity, 2.10×10^7 cm/s at the same electric field. The maximum drift velocity of the hole in this work is 3.17×10^6 cm/s at 1 MV/cm.

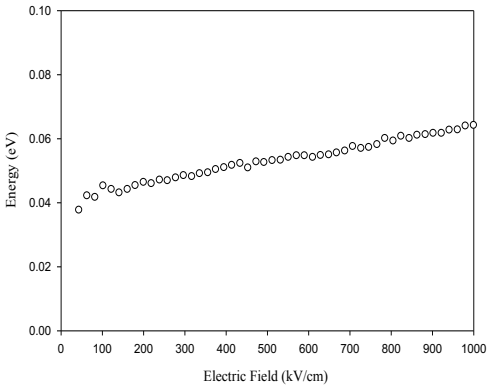

Fig. 5 $Al_{0.45}Ga_{0.55}N$ hole energy as function of electric field.

Fig. 5 plots the average hole energy of $Al_{0.45}Ga_{0.55}N$ as a function of electric field in our work. It is evident that the average hole energy is much lower than the average electron energy. The average hole energy increases slowly from 0.04 eV to 0.065 eV when the electric field increases from 50 kV/cm to 1 MV/cm.

The hole occupancy of $Al_{0.45}Ga_{0.55}N$ as a function of electric field is plotted in Fig. 6. It is shown that all the holes reside on the first valence valley which is the heavy band due to the hole being too heavy to move to the second valence valley which is the light band.

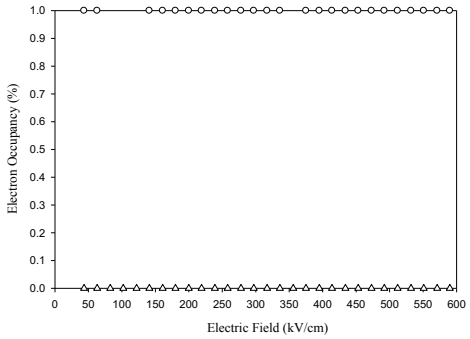

Fig. 6 $Al_{0.45}Ga_{0.55}N$ hole occupancy as function of electric field. Circle: Occupancy of hole at first valley. Triangle: Occupancy of hole at second valley.

Fig. 7 and Fig. 8 show the impact ionization rate as a function of impacting carrier energy of both electron and hole, respectively, for $Al_{0.45}Ga_{0.55}N$ in our work. There is very limited result on impact ionization rate for $Al_{0.45}Ga_{0.55}N$ especially on hole. Since the result of impact ionization rate of $Al_{0.45}Ga_{0.55}N$ cannot be found, it is compared with the closest Al content which is $Al_{0.4}Ga_{0.6}N$ and $Al_{0.5}Ga_{0.5}N$. So far, only Bellotti *et al.*'s (2012) work on electron impact ionization rate can be found. A power exponent of 6 is used in the modified Keldysh formula to generate the impact ionization rate in the first and second conduction valley in our model while a power exponent of 7 is used for the first and second valence valley. It is shown that the impact ionization rate at higher energy valley is higher compared to the lower energy valley especially at a high impact energy. This is due to the larger amount of energy possessed by the carriers at the higher valley. It is also noted that the hole impact ionization rate is higher than of electron.

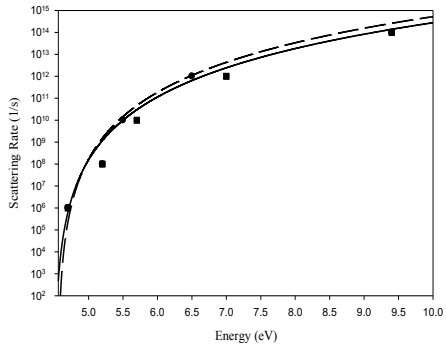

Fig. 7 The electron impact ionization rate as a function of impacting carrier energy for $Al_{0.45}Ga_{0.55}N$. The solid and dashed lines are the ionization rates from the first and second conduction valleys respectively. The circle ($Al_{0.4}Ga_{0.6}N$) and square ($Al_{0.5}Ga_{0.5}N$) represents the ionization rate by Bellotti *et al.* (2012) on the first conduction valley.

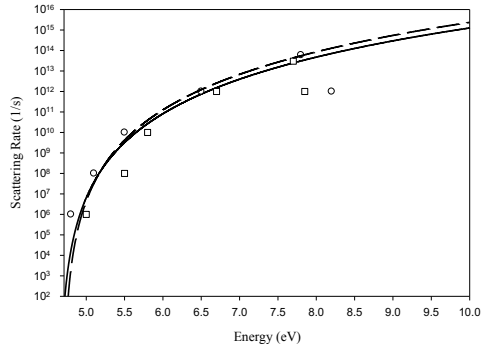

Fig. 8 The hole impact ionization rate as a function of impacting carrier energy for $Al_{0.45}Ga_{0.55}N$. The solid and dashed lines are the ionization rates from the first and second valence valleys respectively. The circle ($Al_{0.4}Ga_{0.6}N$) and square ($Al_{0.5}Ga_{0.5}N$) represents the ionization rate by Bellotti *et al.* (2012) on the first valence valley.

The electron and hole impact coefficients were simulated as a function of inverse electric field by using Eqs. (7) and (8) and are plotted in Fig 9. From our result, it is seen that the hole dominates the impact ionization above the electric field of 2.6 MV/cm. At lower electric field however, electron dominates the impact ionization. The hole domination at higher electric field is consistent with the literature reviews (Huang *et al.*, 2013; Bellotti *et al.*, 2012; Hou *et al.*, 2015). The disparity of α and β values are important as it will give us a low noise while having a high gain APD. From our work, it can be seen that the disparity between α and β is quite small at lower electric field which will result in higher noise. This ratio of noise to gain will progressively decreases after the electric field of 2.6 MV/cm when the value of α and β start to have larger disparity. As impact ionization coefficient for $Al_{0.45}Ga_{0.55}N$ cannot be found, the closest $Al_{0.4}Ga_{0.6}N$ is chosen from other researchers to compare our result. Our electron impact ionization result is very close to the result from Bulutay (2002) and Bellotti *et al*. (2012) and our hole impact ionization is also close to Bellotti *et al*. result. Our results agree where the value of β is higher than α at higher electric field from both the result from Bellotti *et al*. and Tut *et al*. (2006). However, the both of the coefficient from Tut *et al*. is much higher than our result, though this might be due to the lattice defect in the AlGaN layer explained in Tut *et al*. work. Comparing our work with Cheang *et al.* (2019) GaN impact ionization coefficient, it can be seen that both α and β values of $Al_{0.45}Ga_{0.55}N$ are lower than that of GaN. For GaN, hole dominate the impact ionization at lower field compared to electron domination for $Al_{0.45}Ga_{0.55}N$. Since the hole dominates at higher field for $Al_{0.45}Ga_{0.55}N$, it can be assumed that hole will lead the gain for $Al_{0.45}Ga_{0.55}N$ where the breakdown voltage for hole will be lower than electron. This will also mean that most of the noise from $Al_{0.45}Ga_{0.55}N$ will result from electron-initiated impact ionization (Bellotti *et al.*, 2014). Based on the impact ionization coefficients in Fig. 9, the electric field dependent expressions of electron and hole impact ionization coefficients have been deduced as

$$\alpha = 1.66\times10^{7}\exp\left[-\left(\frac{8.51\times10^{8}}{E}\right)^{1.75}\right] \text{ cm}^{-1} \quad (9)$$

$$\beta = 8.01\times10^{7}\exp\left[-\left(\frac{1.02\times10^{9}}{E}\right)^{1.65}\right] \text{ cm}^{-1} \quad (10)$$

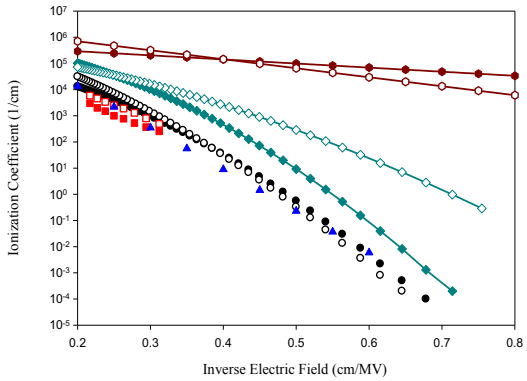

Fig. 9 Electron impact ionization coefficient, α (filled black circle) and hole impact ionization coefficient, β (empty black circle) of $Al_{0.45}Ga_{0.55}N$ from this work are compared with those by Bellotti *et al.* (2012) $Al_{0.4}Ga_{0.6}N$ (α: filled red square, β: empty red square), Tut *et al.* (2006) $Al_{0.4}Ga_{0.6}N$ (α: filled maroon hexagon, β: empty maroon hexagon), Bulutay (2002) $Al_{0.4}Ga_{0.6}N$ (α: blue triangle), Cheang *et al.* (2019) GaN (α: filled teal diamond, β: empty teal diamond).

CONCLUSION

In this work, the carrier transport mechanisms for $Al_{0.45}Ga_{0.55}N$ were investigated using Monte Carlo (MC) simulation. Both the electron and hole coupled with two conduction and valence band, respectively, were simulated. The carrier drift velocity, energy, and carrier occupancy with respect to electric field were simulated. The impact ionization rate and coefficient of both electron and hole were also presented. Our drift velocity for electron is comparable to other literature result while no literature review for the hole drift velocity. At the electric field of 170 kV/cm, the electron gains enough energy to be excited to the second valley, maintaining a 40 – 60 ratio of first valley to second valley respectively above the electric field of 560 kV/cm. The hole impact ionization rate is higher than that of electron. The hole dominates the impact ionization process above the electric field of 2.6 MV/cm and vice versa as seen in the impact ionization coefficient figure. The impact ionization coefficient will be used to calculate the gain and noise of our model in our future work where we predict that hole will have higher multiplication gain compared to electron and electron-initiated multiplication will have higher noise factor than holes.

ACKNOWLEDGEMENT

This work was supported by MMU/RMC-PL/FRGS/AL/2017/033, MoHE.

REFERENCES

Tsao, J. Y., Hollis, M. A., Kaplar, R. J. 2017. Ultrawide-bandgap semiconductors: Research opportunities and challenges. *Adv. Electron. Mater.,* 1600501.

Kaplar, R. J., Allerman, A. A., Armstrong, A. M., Crawford, M. H., Dickerson, J. R., Fischer, A. J., Baca, A. G., Douglas, E. A. 2017. Review-Ultra-wide-bandgap AlGaN power electronic devices. *ECS J. Solid State Sci. Technol.*, *6*(2), Q3061-Q3066.

Monroy, E., Omnès, F., Calle, F. 2003. Wide-bandgap semiconductor ultraviolet photodetectors. *Semicond. Sci. Technol*., *18*(4), R33.

Huang, Z., Li, J., Zhang, W., Jiang, H. 2013. AlGaN solar-blind avalanche photodiodes with enhanced multiplication gain using back-illuminated structure. *Appl. Phys. Exp*., *6*(5), 054101, 1-4.

Qu, J., Li, J., Zhang, G. 1998. AlGaN/GaN heterostructure grown by metalorganic vapor phase epitaxy. *Solid State Commun., 107*(9), 467-470.

Dong, K. X., Chen, D. J., Jin, B. B., Jiang, X. H., Shi, J. P. 2016. $Al_{0.4}Ga_{0.6}N/Al_{0.15}Ga_{0.85}N$ seperate absorption and multiplication solar-blind avalanche photodiodes with a one-dimensional photonic crystal filter. *IEEE Photon. Journal*, *8*(4), 1-7.

Yuan, P., Anselm, K. A., Hu, C., Nie, H., Lenox, C., Holmes, A. L., Streetman, B. G., Campbell, J. C., McIntyre, R. J. 1999. A new look at impact ionization—Part II: Gain and noise in short avalanche photodiodes. *IEEE Trans. Electron Devices.*, *46*(8), 1632-1639.

Farahmand, M., Garetto, C., Bellotti, E., Brennan, K. F., Goano, M., Ghillino, E., Ghione, G., Albrecht, J. D., Ruden, P. P. 2001. Monte Carlo simulation of electron transport in the III-Nitride wurtzite phase materials system: Binaries and ternaries. *IEEE Trans. Electron. Devices, 48*(3), 535-542.

El-Ela, F. M. A., Mohamed, A. Z. 2013. Electron transport characteristics of wurtzite GaN. *ISRN Condensed Matter. Phys.*, *2013*, 654752.

Bellotti, E., Bertazzi, F. 2014. Numerical simulation of deep-UV avalanche photodetectors. *Proc. SPIE 8980, Physics and Simulation of Optoelectronic Devices XXII*, 8980, 89800R.

Tomizawa, K. 1993. Numerical simulation of submicron semiconductor device. *London: Artech House.*

Lee, S. R., Wright, A. F., Crawford, M. H., Petersen, G. A., Han, J., Biefeld, R. M. 1999. The band gap of AlGaN alloys. *Appl. Phys. Lett.*, *74*, 3344.

Zhang, J., Guo, L. W., Chen, Y., Xu, P. Q., Ding, G. J., Peng, M. Z., Jia, H. Q., Zhou, J. M., Chen, H. 2009. Growth and characteristics of epitaxial $Al_xGa_{1-x}N$ by MOCVD. *Chinese Phys. Lett.*, *26* (6), 068101.

Dridi, Z., Bouhafs, B., Ruterana, P. 2002. First-principles calculation of structural and electronic properties of wurtzite $Al_xGa_{1-x}N$, $In_xGa_{1-x}N$, and $In_xAl_{1-x}N$ random alloys. *Phys. Stat. Sol. (c)*, *0*(1), 315-319.

González, R. N., Serrato, A. R., Amarillas, A. P., Galvan, D. H. 2008. First-principles calculation of the band gap of $Al_xGa_{1-x}N$ and $In_xGa_{1-x}N$. *Rev. Mex. Fıs*., *54* (2), 111-118.

Joachim, P. 2007. Nitride Semiconductor Devices: Principle and Simulation. *Portland Wiley-VCH.*

Angerer, H., Brunner, D., Freudenberg, F., Ambacher, O., Stutzmann, M., Hopler, R., Metzger, T., Born, E., Dollinger, G., Bergmaier, A., Karsch, S., Korner, H. J. 1997. Determination of the Al mole fraction and the band gap bowing of epitaxial $Al_xGa_{1-x}N$ films. *Appl. Phys. Lett.*, *71*(11), 1504.

Yun, F., Reshchikov, M. A., He, L., King, T., Hadis, M., Steve, W. N., Wei, L. C. 2002. Energy band bowing parameter in $Al_xGa_{1-x}N$ alloys. *J. Appl. Phys*., *92*(8), 4837-4839.

Stutzmann, M., Ambacher, O., Angerer, H., Nebel, C. E., Rohrer, E. 1998. Electrical and structural properties of AlGaN: A comparison with CVD diamond. *Diamond and Related Materials, 7*(2–5), 123-128.

Coltrin, M. E., Baca, A. G., Kaplar, R. J. 2017. Analysis of 2D transport and performance characteristics for lateral power devices based on AlGaN alloys. *ECS Journal of Solid State Science and Technology, 6* (11), S3114-S3118.

Keldysh, K. V. 1965. Concerning the theory of impact ionization in semiconductor. *Soviet Phys. JETP, 21*(6), 1135-1144.

You, A. H., Cheang, P. L. 2008. Effect of doping concentration on avalanche multiplication and excess noise factor in submicron APD. *Microelectronics Reliability, 48,* 547-554.

Morkoç, H. 2008. Handbook of Nitride Semiconductors and Devices: Materials Properties, Physics and Growth, *Volume 1*, *Weinheim: Wiley-VCH Verlag GmbH & Co. KGaA*.

Bulutay, C. 2002. Electron initiated impact ionization in AlGaN alloys. *Institute of Physic Publishing, Semiconductor Science and Technology, 17* (10), 59-62.

Litvinov, V. I. 2003. Electron spin splitting in polarization-doped group-III nitrides. *Phys. Rev. B, 68*, 155314.

Anwar, A. F. M., Wu, S., Webster, R. T. 2001. Temperature dependent transport properties in GaN, $Al_xGa_{1-x}N$, and $In_xGa_{1-x}N$ semiconductors. *IEEE Trans. Electron. Devices, 48* (3), 567-572.

Bachir, N., Hamdoune, A., Sari, N. E. C. 2012. Electrical transport in ternary alloys: AlGaN and InGaN and their role in optoelectronic. *InTech Semiconductor Laser Diode Technology and Applications*, *2,* 13-28.

Yarar, Z., Ozdemir, M. 2010. Alloy scattering dependence of electron transport in AlGaN. *Balk. Phys. Lett.*, *18*(181031), 237-242.

Bellotti, E., Bertazzi, F. 2012. A numerical study of carrier impact ionization in $Al_xGa_{1-x}N$. *J. Appl. Phys., 111*, 103711.

Hou, M., Qin, Z., He, C., Wei, L., Xu, F., Wang, X., Shen, B. 2015. Study on AlGaN p-i-n-i-n solar-blind avalanche photodiodes with $Al_{0.45}Ga_{0.55}N$ multiplication layer. *Electron. Mater. Lett., 11*(6), 1053-1058.

Tut, T., Gokkavas, M., Butun, B., Butun, S., Ulker, E., Ozbay, E. 2006. Experimental evaluation of impact ionization coefficients in $Al_xGa_{1-x}N$ based avalanche photodiodes. *Appl. Phys. Lett., 89*, 183524.

Cheang, P. L., Wong, E. K., Teo, L. L. 2019. Avalanche characteristics in thin GaN avalanche photodiodes. *Jpn. J. Appl. Phys*., *58*, 082001.